LIMNOLOGY
and
OCEANOGRAPHY

Limnol. Oceanogr. 00, 2017, 00–00

doi: 10.1002/lno.10522

Wind and buoyancy driven horizontal exchange in shallow embayments of a tropical reservoir: Lake Argyle, Western Australia

B. L. Woodward,[1]* C. L. Marti,[2] J. Imberger,[3] M. R. Hipsey,[4] C. E. Oldham[1]

[1]School of Civil, Environmental and Mining Engineering, The University of Western Australia, Crawley, Western Australia, Australia
[2]Sustainable Engineering Group, Faculty of Science and Engineering, Curtin University, Bentley, Western Australia, Australia
[3]Rosenstiel School of Marine and Atmospheric Science, University of Miami, Coral Gables, Florida
[4]School of Earth and Environment, The University of Western Australia, Crawley, Western Australia, Australia

Abstract

Many factors including depth, vegetation density, wind, and gyres may act to influence the littoral exchange in a water body but very few studies have investigated the interaction between more than two of these factors at any time. To investigate these controls on horizontal exchange in a large tropical reservoir, we conducted a 9-d intensive field experiment in Lake Argyle, Western Australia. The experiment began with a 7-d cooling period that generated water in the shallows of the reservoir embayments that was persistently cooler than the interior. This led to an underflow of dense water that moved from the lake boundary toward the center of the reservoir. A three-dimensional hydrodynamic model (ELCOM) was able to adequately reproduce this thermal structure and was used to demonstrate its sensitivity to wind-sheltering effects and submerged macrophyte presence. Further analysis of the predictions indicated that when the ratio of the shear and buoyancy force, averaged over 6 h (B_{6h}) and 6-h averaged wind speed in the direction of the embayment (U_{6h}) was (1) greater than 0.5 ms^{-1} and 4.5 ms^{-1} respectively, the exchange was dominated by a topographic gyre formation, (2) when $0.1 < B_{6h} < 0.5$ and 2.4 ms$^{-1} < U_{6h} < 4.5$ ms^{-1}, the resulting circulation was a combination of differential cooling flows and a topographic gyre circulation, and (3) when U_{6h} fell below 2.4 ms^{-1}, purely buoyancy driven flow occurred but only if the buoyancy forces across the embayments were an order of magnitude greater than wind-induced velocity shear.

Spatial gradients of constituents such as dissolved oxygen and nutrients periodically develop between the littoral and pelagic waters of large lakes and reservoirs, which, depending on the rate of water exchange, can result in large fluxes of these constituents from the lake boundary to the interior, or interior to the lake boundary (Marti and Imberger 2008; Tanino 2012). An understanding of this exchange is critical to quantify ecological and biogeochemical processes in lakes and reservoirs such as primary production, greenhouse gas evasion and the transport of pollutants. The stress imposed by the wind on the water surface is typically the dominant force that drives the exchange, but under calm conditions or in embayments sheltered from the wind, horizontal density gradients created by differential heating and cooling create a body force across the lake leading to a buoyancy driven flow (Tanino 2012). However, the degree to which these forces compete and/or interact with each other, particularly as they may be out of phase during natural meteorological forcing, remains uncertain.

Previous studies exploring littoral exchange have been conducted in thermally stratified water bodies where internal waves (Lorke et al. 2006, 2008; Marti and Imberger 2008), benthic boundary layer transport (Marti and Imberger 2006), and upwelling in the littoral zone (Monismith et al. 1990; Rueda et al. 2003; Rueda and Cowen 2005; Macintyre et al. 2014) also influenced mixing near the shoreline. Studies exploring exchange in tropical water bodies, which is the focus of this study, have been comparatively rare relative than to those undertaken in temperate zones, and Rueda et al. (2003) also noted a lack of studies on well-mixed lakes. Within tropical lakes, the above-mentioned mechanisms are not likely to be important during the cool season, rather vertical mixing is expected (Lewis 1996), possibly followed by a thermal structure influenced by density currents generated by differential cooling (Talling and Lemoalle 1998). This therefore makes tropical lakes during the cool season an interesting case study to explore buoyancy-induced flows.

*Correspondence: bronwyn.woodward@research.uwa.edu.au

Spatial temperature differences arising from heating or cooling of variable depth water have been commonly identified as the cause of density-driven currents in lakes and reservoirs (Peeters et al. 2003). When the net heat flux acting on a lake surface is negative, the shallower littoral zones cool more quickly than the deeper offshore waters. The colder, denser water in the littoral zone then falls by gravitational adjustment down the sloping bottom. In response, warmer surface water is drawn across the surface from the lake interior toward the littoral zone (Imberger 1985). A reverse circulation pattern occurs during differential heating.

Horizontal temperature gradients can also emerge due to differences in light extinction and shading caused by aquatic vegetation (Lövstedt and Bengtsson 2008), differential absorption due to variable turbidity (MacIntyre et al. 2002), groundwater inflow (Roget et al. 1993), and wind sheltering (Monismith et al. 1990) or spatial differences in meteorology across lakes larger than 10,000 km^2 (Verburg et al. 2011; Macintyre et al. 2014). Emergent vegetation in the shallows can significantly alter circulation patterns by reversing or reducing the horizontal temperature gradients that occur due to variation in water depth. Vegetation may cause differential cooling during the day due to shading (Lin and Wu 2015) and reduce radiation losses and differential cooling at night (Pokorný and Květ 2004).

Aside from influencing the surface heat budget, wind stress acting across the surface of a non-rotating lake drives a water current in the same direction as the wind, that decays with increasing depth and eventually reverses in direction near the lake boundary, due to the return flow generated by conservation of mass (Tanino 2012). This circulation pattern can be similar to that generated by differential heating or cooling so that when the wind stress acts in the same direction as the thermally driven gravity current, it increases the flow speeds; conversely wind stress in the opposite direction can easily change the structure of the underlying thermally driven circulation (Tanino 2012). Wind-driven gyres may also form depending on interactions of the flow with lake boundary and influence circulation in lake embayments (Razmi et al. 2013) and net exchange. Both the thermally driven exchange flow (Zhang and Nepf 2009), and surface wind-driven circulation (Lin 2015), may be inhibited by vegetation drag. Although many factors including water depth, vegetation density, wind, and gyres may act together to influence the littoral exchange in a lake, very few studies have investigated the interaction between more than two of these at any time.

Numerical modelling has estimated that the velocity of density currents generated by density differences in reservoir sidearms may be as high as 0.1 ms^{-1} (Farrow and Patterson 1994), and this is typically the order of maximum velocities of density currents measured in lakes and reservoirs in the field (Monismith et al. 1990; Nepf and Oldham 1997; George 2000; Rueda et al. 2003). Previous estimates of the velocity of wind-generated currents (based on expected ratios of water velocity to wind speed) indicate that they will usually be stronger than thermally driven currents (Macintyre et al. 2014). Assuming surface drift velocities are approximately 2% of wind speeds in the absence of vegetation drag (Wetzel 2001), even a gentle breeze of 5 ms^{-1} should create currents stronger than those generated by differential heating and cooling in most lakes and reservoirs. However, mathematical solutions of an idealized system, under laminar flow conditions within a region of homogeneous sparse vegetation suggested wind speeds more than double this are required to override the underlying thermally driven circulation (Tanino 2004). The behavior of the flow at intermediate wind stress is less well understood, but the same analytical analysis predicted a three-layered flow structure for opposing wind speeds of 6.5 ms^{-1} where the wind only reverses the direction of the density flow at the surface (Tanino 2004). Rattray and Hansen (1962) suggested that weaker winds might only decrease the surface and bottom velocities without changing the direction of the flow. However, the effect of wind is not constant across the whole lake mainly because the aerodynamic effects of topography. While these spatial variations in the wind field may play a key role in determining circulation patterns and flushing times of different areas of a lake, few studies have explored their impact (Rueda et al. 2005; Marti and Imberger 2008).

Furthermore, most numerical analyses and field studies have focused on diurnal forcing such as night-time cooling, daytime heating, or sea breeze patterns, as a driver for exchange between the littoral zone and the interior of lakes and reservoirs, but differential heating and cooling and variations in wind patterns have also been observed to occur in lakes over synoptic times scales (Andratottir and Nepf 2001). The strength of convective exchange in a reservoir embayment was found to depend on the net daily heat flux and the heat flux over previous days, suggesting that convective exchange patterns may be regulated, in part, by weather patterns that result in general warming and cooling trends (James et al. 1994). Curtarelli et al. (2014) found that differential cooling in a tropical reservoir was intensified over a period of several days due the passage of cold fronts. These studies highlight that it is important to examine these processes over timescales longer than a day.

One of the challenges in exploring the range of flows that occur within a lake at the right spatial and temporal scales to adequately understand the exchange between the littoral zone and interior is the lack of high-resolution sampling data (Rueda et al. 2003), and therefore hydrodynamic models are able to fill the gaps in the observational data (Rueda and Schladow 2003; Marti and Imberger 2008; Curtarelli et al. 2014). Two-dimensional numerical analyses of buoyancy-driven flows have incorporated unsteady forcing and interacting forces such as wind (Farrow 2012), as well as vegetation shading and drag (Lin 2015). These models have provided considerable insight into wind- and buoyancy-driven circulation over both vegetated and unvegetated slopes within triangular domains but have limitations when translating the results to lakes with more complex morphometry. More realistic geometric representations of reservoirs have further advanced understanding of natural convection in nearshore regions (Yu et al. 2015) but two-dimensional models are unable to include the effect of three-dimensional (3D) variation in lake bathymetry that can influence the wind-driven circulation patterns, gyre formation and flushing times within lake embayments (Razmi et al. 2013). 3D models can therefore provide further insights in understanding the dynamics of natural systems, but to date there have been limited analyses using 3D models to capture the interplay between the numerous factors that influence littoral exchange over a range of timescales relevant to lake management.

This study aims to define critical wind speeds at which wind stress or buoyancy forces become the dominant force responsible for driving horizontal exchange between the embayments and the interior of a tropical reservoir with complex topography and a vegetated littoral zone. Water column thermal structure and meteorological data were collected at the reservoir interior and vertical temperature profiles were collected within the embayments and reservoir interior. This data were combined with high spatial and temporal resolution temperature and velocity data from a 3D hydrodynamic model to investigate a cooling period in May–June 2012. The model data were used to determine the significance of buoyancy-driven exchange compared to wind-driven exchange and gyre formation, as a function of increasing wind speed and direction. Model scenarios with and without reduced wind to account for wind sheltering, the effect of vegetation shading and vegetation drag in the littoral zone allowed us to assess how these attributes modify the relative importance of buoyancy and wind forces for the exchange. Finally, we compared the model performance for each of these scenarios to highlight factors that should be considered when modelling lakes and reservoirs with large shallow regions and sheltering from surrounding topography.

Methodology

Study site

Lake Argyle is a tropical reservoir located in the north of Western Australia, Australia, between 16°S and 16.7°S (Fig. 1) with a surface area of 980 km^2 at full supply level (FSL, $\sim$ 92.2 m above sea level, ASL). The reservoir was created by the damming of the Ord River in 1971 and has a maximum depth of 51 m in the flooded river canyon near the dam wall but many extensive shallow embayments and a mean depth of only 10.1 m at FSL. Large beds of the macrophytes *Potamogeton* sp. and *Hydrilla* sp. have been observed in the littoral regions of the reservoir (Kimberley Aquaculture Development Strategy ... 1999) and were also observed during our field study. There is a small mountain range on the western side of the reservoir with an average elevation of approximately 250 m ASL and a maximum elevation of approximately 500 m ASL. The topography around the rest of the lake is flatter with an average elevation of less than 150 m ASL and only a few small peaks of less than 400 m ASL.

The climate at the reservoir is classified as arid and hot steppe (Peel et al. 2007) and our field study was conducted in May–June, a time of high water levels and cooling in the reservoir. The influence of the Asian-Australian monsoon causes a warm, wet season between December and March which is followed by a dry, relatively cool season affected by strengthening south-east trade winds between April and August (www.bom.gov.au [accessed 23 May 2016]). Differential cooling and the resulting horizontal temperature gradients occur in the reservoir at the start of the dry season (April to June) because of the cooler conditions (Imberger 1977). This is also one of the windiest times of the year. Our field investigation followed a wet season with average rainfall, resulting in reservoir water levels $\sim$ 0.3 m above FSL level at the start of the field experiment ($\sim$ 92.5 m ASL); these high water levels created extensive shallow littoral zones. These conditions made Lake Argyle an ideal study site to explore the interplay between buoyancy-induced flows vs. shear-induced.

Field measurements

A Lake Diagnostic System (LDS, Imberger 2004) was installed in May 2011 in the middle of the Ord river channel (depth $\sim$ 31.5 m) approximately 22 km upstream of the dam wall (16.31°S, 128.68°E) (Fig. 1). Data on the water column thermal structure, water level and meteorology were collected every 20 s. The LDS consisted of one floating and one bottom-mounted thermistor chain equipped with a total of 20 thermistors measuring water column temperature from 0.7 m below the water surface to 1 m above the reservoir bottom, at depths intervals that varied from 1 m to 4 m, a pressure (depth) sensor (located 5 m from the reservoir bottom) and a surface meteorological station measuring air temperature, wind speed and direction, relative humidity, incoming short wave radiation, and net total radiation, at approximately 2 m above the water surface. Data from the bottom four thermistors of the floating chain were not used because they were either not functioning or overlapped the bottom-mounted chain.

Additionally, an intensive field study was conducted over 9 d, from 24 May to 01 June 2012 where profiling was conducted using the Portable Flux Profiler (PFP, Machado et al. 2014). The PFP included a fine scale profiler that measured pressure, temperature, conductivity, dissolved oxygen, pH, photosynthetic active radiation (PAR), and turbidity

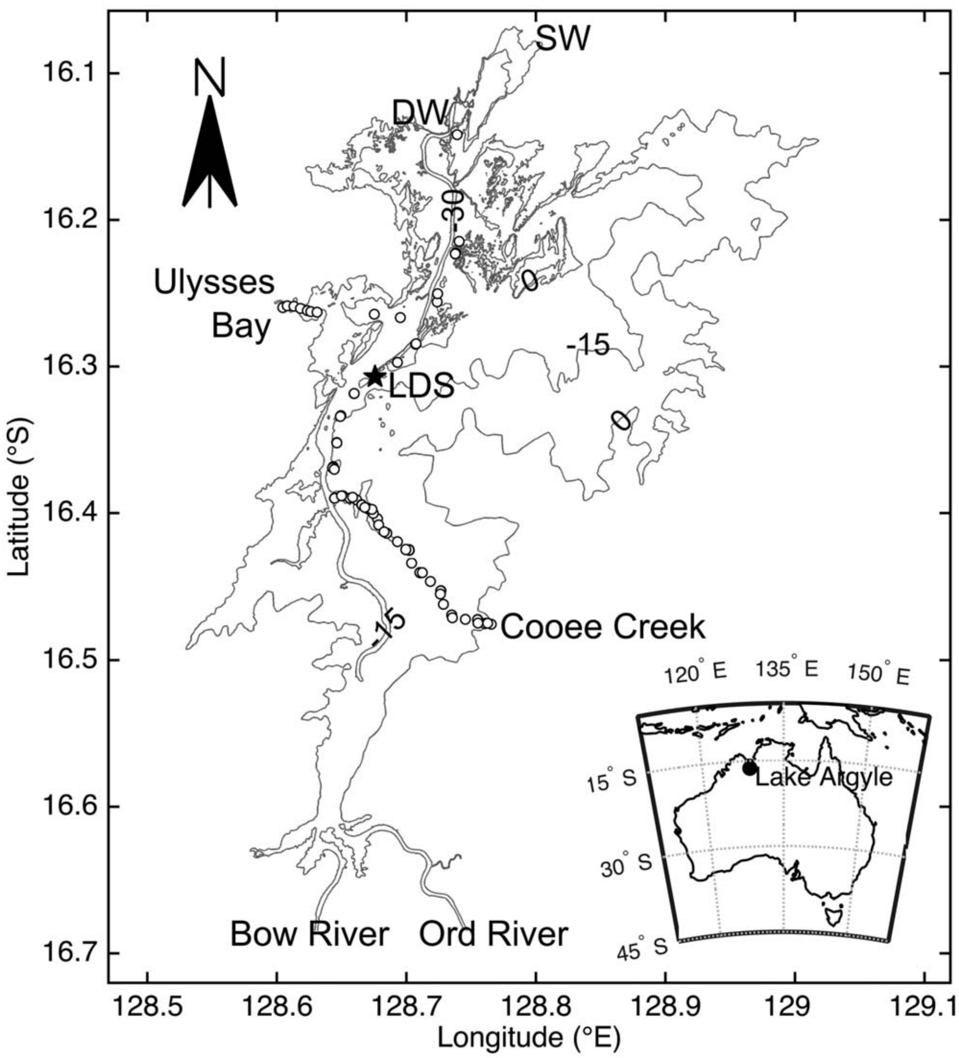

Fig. 1. Location and bathymetry of Lake Argyle. Isobaths are given every 15 m from 0 m to 30 m depth. The Ord River and one of its tributaries, the Bow River, both located to the south, are the major inflows while a spillway (SW) and hydropower and controlled releases at the dam wall (DW) drain the reservoir to the north. Circles indicate mobile PFP profile locations. The position of the Lake Diagnostic System (LDS) is indicated by a star and was also used as a profile location.

(Imberger and Head 1994). The PFP also measures profiles of water velocity, however the sensor was not functioning correctly and the data were not included in this analysis. A total of 287 profiles were collected along transects that followed the drowned creek channels in eight reservoir embayments and into the main Ord River channel, with some additional profiles collected to characterize the shallow areas of the embayments (Fig. 1). This paper focuses primarily on the Cooee Creek embayment and Ulysses Bay, which were aligned almost in the opposite directions. Cooee Creek was profiled on four occasions over the last 5 d of the experiment while the other embayments were only profiled over a single day.

The PFP was deployed in free fall mode with a fall velocity of approximately 0.1 ms^{-1} and the fine scale variables were sampled at 50 Hz, yielding measurements in the vertical approximately every 2 mm. Only the fine-scale temperature measurements are described in detail in this paper. The fine-scale temperature and conductivity signals were sharpened and matched for the response times of the sensors according to Fozdar et al. (1985). Data were discarded from the top 0.2 m and bottom 0.05 m of each profile, and when the fall velocity was less than 0.02 ms^{-1}.

Surface energy fluxes

The effective heat flux into the surface layer (F_s) was estimated by difference using net total radiation (R_n) and latent (E) and sensible (H) heat fluxes:

$$F_s = R_n - E - H \tag{1}$$

R_n was measured at the LDS and E and H were estimated via bulk aerodynamic methods with adjustment of the transfer coefficients for non-neutral atmospheric stability (Verburg and Antenucci 2010). A cutoff of $|\zeta| < 15$ was imposed during the computation of the stability parameter (ζ) (Imberger and Patterson 1990; MacIntyre et al. 2002). The numerical hydrodynamic model ELCOM, described in the next section, used the same method to adjust the bulk-transfer coefficients.

Numerical simulations

Numerical simulations were performed using the 3D Estuary, Lake and Coastal Ocean Model (ELCOM). The model adopted a z-coordinate Cartesian grid to solve the unsteady Reynolds-averaged Navier–Stokes Equation using the Boussinesq approximation and hydrostatic assumption (Hodges et al. 2000). Temperature was modelled using the ULTIMATE-QUICKEST numerical scheme for transport (Leonard 1991), with additional sub-model components for surface heating and vertical mixing. This approach has been demonstrated to accurately predict the velocity structure (Marti and Imberger 2008) and thermal structure in a wide variety of lakes and reservoirs (Chung et al. 2009; Leon et al. 2012; Marti et al. 2016).

Bathymetry and computational domain

The bathymetry of Lake Argyle was digitized from 5 m bathymetric contours (Public Works Department … 1982) that had been interpolated from land elevation data derived from aerial photographic images taken before the reservoir was flooded. A sedimentation survey of Lake Argyle in 2006 (Dixon and Palmer 2010) estimated that 5% of the reservoir had been filled with sediment since its construction. Most of this sediment has been deposited along the mid to upper reaches of the flooded Ord River channel, 25–64 km from the dam wall, and the channel has been completely filled from 38 km to 55 km from the dam wall (Dixon and Palmer 2010). Depth measurements recorded during our profiling were consistent with the findings of the 2006 survey.

ELCOM was applied to Lake Argyle using a uniform horizontal grid of 250 m and uniform vertical resolution of 0.25 m. The horizontal grid size was larger than the width of the upstream sections of the submerged river channels in the embayments, which are less than 50 m wide, but it was a practical compromise considering available computing power. The bathymetry was modified to ensure the main river and creek channels were included and their depth matched recent field observations.

Model setup

The simulation was started on midday 21 May 2012, 2.5 d before the period of interest, to spin up the water temperature gradient and circulation patterns, and ran to the end of 01 June 2012. A time-step of 300 s was adopted to satisfy the Courant–Friedrichs–Lewy (CFL) condition (Courant number < 1) for maximum horizontal water velocities expected in the reservoir, but not for internal waves (Hodges and Dallimore 2013); these were not expected during the simulation period because the reservoir was not strongly stratified. The vertical temperature gradient recorded by the LDS was typically below 0.05°C m^{-1} and never above 0.5°C m^{-1}. Data collected by the LDS thermistor chain were used as the initial temperature profile, which was applied uniformly across the domain. A uniform initial salinity of 0.134 psu was assumed based on profile data collected on 21 May 2012. A numerical tracer was introduced once, on the first time-step of the 24$^{\text{th}}$ May, to computational cells in the embayments with a depth of less than 5 m. The temporal changes in tracer concentrations were used to examine the movement of water out of the embayments during the field experiment.

The simulation was initially carried out using mostly default model parameters, which were based on non-site-specific literature values (Hodges and Dallimore 2013) (Table 1). As described above, the bulk-transfer parameters used within the surface thermodynamics module were corrected to account for the effects of non-neutral atmospheric stability. In the first model run (Scenario 1), the light extinction coefficient was set to 2.5 m^{-1} near the inflows, and set to the default of 0.89 m^{-1} for the rest of the domain (Table 1); this was based on interpretation of profiles of PAR collected during the field experiment. The default model value of 5.0×10^{-3} was used for the dimensionless bottom drag coefficient which is comparable to values expected for rougher bed types such as gravel or rippled sand (Johns 1983) but similar values for have been observed in water-bodies with silty beds (Ali and Lemckert 2009) so this value is not considered unreasonable for the silty clay sediment of Lake Argyle (Dixon and Palmer 2010).

Forcing conditions

The model was forced with meteorological data from the LDS, including short wave radiation, calculated net long wave radiation, air temperature, relative humidity, wind (speed and direction), which were applied uniformly across the reservoir domain. There was no rainfall during the field experiment. The model was also forced with inflows from the Ord and Bow Rivers calculated from daily inflows recorded at three upstream flow-monitoring stations, outflow over the spillway calculated from daily measurements of reservoir levels and a rating curve, and measurements of hydropower and regulated releases provided by the Water Corporation. The inflow rate from the Ord and Bow Rivers was 12.5 m^3 s^{-1} or less during the field experiment, which was less than one tenth of the estimated rate of wind and buoyancy driven exchange between the largest reservoir embayment and the interior. The daily inflow volume was less than 0.02% of the lake volume and the river inflows are also located more than 20 km from the embayments. Therefore, during the timeframe of this study the river flows are not expected to have an impact on the circulation within the embayments. Due to the lack of in situ data, a simple

Table 1. Parameters used for ELCOM simulation.

Parameter		Unit	Value
Mean albedo for short-wave radiation		-	0.08
Mean albedo for long-wave radiation		-	0.03
Extinction coefficient for photosynthetically active radiation (PAR)		m^{-1}	0.89–2.5
Extinction coefficient for near infrared radiation		m^{-1}	1
Extinction coefficient for ultraviolet A wavelength		m^{-1}	1
Extinction coefficient for ultraviolet B wavelength		m^{-1}	2.5
Bulk transfer coefficient for heat at air-water interface		-	1.3×10^{-3}
Bulk transfer coefficient for momentum at air-water interface		-	1.3×10^{-3}
Mixing coefficients for:	- wind stirring	-	1.33
	- bottom generation of turbulent kinetic energy (TKE)	-	2.2
	- shear generation of TKE	-	0.15
	- energy generated from convective overturn	-	0.2
	- dissipation of excess energy	-	1.15
Bottom drag coefficient		-	5.0×10^{-3}
Sediment reflectivity (proportion of excess short-wave radiation at the bottom of a column of water reflected back into the domain)		-	0.9
Extinction coefficient for short-wave radiation reflected from bottom		m^{-1}	2.5

3-d moving average of the air temperature recorded at the nearest land-based meteorological station was used to set the boundary condition of temperature at the inflows. The sampling rate of the air temperature at the meteorological station was 30 min. A 3-d moving average of the air temperature provided a better match with the measured inflow temperature and the inflow temperature estimated by heat flux calculations than using a shorter averaging period (e.g., 1 d or 8 h). A constant value of 0.3 psu was used for the inflow salinity, taken from profiles collected near the inflows during the field experiment.

Configuration of different simulation scenarios

In addition to the base set up and forcing described above (Scenario 1), three additional model scenarios were run to assess the model sensitivity to the different physical processes that influence flows into and out of the embayments. First, a wind reduction coefficient of 0.85 was applied to account for wind sheltering by the surrounding topography (Scenario 2). This coefficient was determined by dividing the area of wind access over the lake A_w by the total lake area. The A_w was approximated by the following geometrically based relationship given by Markfort et al. (2010):

$$A_w = \frac{D^2}{2}\cos^{-1}\left(\frac{X\tau}{D}\right) - \frac{X_\tau}{2}\sqrt{D^2 - X_\tau^2} \qquad (2)$$

where D is the equivalent circular diameter of the lake (34.9 km), on the basis of lake surface area, and X_τ is the distance from the shoreline at which wind stress is no longer affected by sheltering. Experiments by Markfort et al. (2010) found $X_\tau \approx 50h_c$, where h_c is the height of the surrounding canopy or topography above the water surface.

The sheltering distance (X_τ) was determined firstly by marking out 47 points at ≈ 2.5 km intervals around the lake perimeter in Google Earth. Then a transect was marked from each point extending either in a north, east, south, or westerly direction away from the lake perimeter, depending on which side of the lake the point was located. The topographic elevations from Google Earth were examined along each transect for a distance of 25 km (≈ 50 times the maximum elevation around Lake Argyle). The peak elevations along each transect were identified, then multiplied by 50 and the distance from the shoreline was subtracted to give preliminary values for the sheltering distance. The maximum sheltering distance along each transect was identified, then averaged which gave a spatially averaged sheltering distance for the lake of 4.01 km. Using this value for X_τ in Eq. 2, it was determined that A_w is ~ 85% of the total lake area.

Shading by macrophytes was then included in a third simulation by increasing the light extinction coefficient to 5 m^{-1} and the albedo of the water surface to 0.5 (dimensionless), in those parts of the reservoir that had a depth of less than 2.5 m and where macrophytes were observed in the field (Scenario 3). In Scenario 4, a dimensionless vegetation drag coefficient of 0.1 was also included in these regions; this coefficient is the upper limit observed in freshwater macrophytes (Sand-Jensen 2003). The vegetation height was set to 2.5 m; the drag was therefore applied across the entire depth of the water column in the domain with macrophytes. The wind reduction coefficient of 0.85 from Scenario 2 was also used in Scenarios 3 and 4.

Assessment of model performance

Regression plots comparing hourly LDS temperatures from each thermistor (T_{observed}) with the equivalent ELCOM estimates at the same time and depths ($T_{\mathrm{simulated}}$) were used as a quantitative indicator of model performance within the lake interior. The average root mean squared error (RMSE) was also used to assess model performance, and was defined as:

$$\mathrm{RMSE}=\frac{\sqrt{\sum_N \left(T_{\mathrm{simulated}}-T_{\mathrm{observed}}\right)^2}}{N} \tag{3}$$

where N is the number of points used in the comparison (3240). The statistical performance indicators were almost identical when comparing hourly data and the highest possible temporal resolution (5 min); hourly data was subsequently used to simplify the analysis.

Shear and buoyancy force calculations

The ratio of surface shear forces to the characteristic buoyancy forces (B) has previously been calculated for a shallow rectangular cavity with differentially heated end walls and also applied in natural estuaries (Cormack et al. 1975) and is defined as:

$$B=\frac{L\tau_0}{h^2(T_{\mathrm{h}}-T_{\mathrm{c}})\beta g}=\frac{\text{shear force}}{\text{buoyancy force}} \tag{4}$$

where L and h are the cavity length and depth, T_{h} and T_{c} are the cold- and hot-end wall temperatures, β is the coefficient of thermal expansion (2.14×10^{-4} °C^{-1}) and g is acceleration due to gravity. To apply this ratio to Lake Argyle, the surface kinematic shear stress $\tau_0=\frac{C_{\mathrm{D}}\rho_{\mathrm{a}}u^2}{\rho_0}$ was used, where C_{D} is the dimensionless neutral water surface drag coefficient = 1.3×10^{-3}, ρ_{a} is the air density = 1.2 kg m^{-3}, u is the wind speed measured at the LDS adjusted to be equivalent to the wind speed 10 m above the lake surface using the power law equation (Spera and Richards 1979) with an exponent of 1/7 (Von Karman 1921) and ρ_0 is the reference water density = 1000 kg m^{-3}.

Equation 4 was used to calculate the ratio of the shear forces and the buoyancy force in the Cooee Creek embayment and Ulysses Bay. Depth-averaged temperatures from model profiles near the shore of the embayments and at the LDS were used as the cold- and hot-end wall temperatures. The depth-averaged model temperature for profiles located at the 2.5 m depth contour along the creek channels in the embayments were used because the temperature at these locations showed a good agreement with the field results (further outlined in the Results section). The temperature data from the model were used in the calculation instead of the field data because of its higher temporal resolution in the embayments. For the Cooee Creek embayment, L was the distance from the shore of the embayment to the LDS following the creek channel (34.75 km). For Ulysses Bay, L was measured from the shore of the embayment to the point where the creek channel met the Ord River channel, just to the north (12 km). For both embayments, h was half the depth at the LDS = 15.65 m. The wind speed was subsampled every 5 min and used to calculate the shear stress; this matched the time-step of the model data that was also used in the calculation. The instantaneous wind speed was used in the calculation instead of a time-averaged value, to allow analysis of fluctuations in the force balance over small time-steps. The component of the wind speed aligned with the direction of the creek channels was used in the calculation.

When $B \gg 1$, the shear forces are expected to dominate and the horizontal exchange between the lake shore and interior can be considered to be forced by wind. When $B \ll 1$, the buoyancy forces are expected to dominate and the problem is equivalent to the case $\tau_0=0$ in Cormack et al. (1975). Nepf and Oldham (1997) used a similar method to compare the magnitude of the shear and buoyancy forces driving exchange flow in the forebay of a shallow wetland. We further quantified the relationship between B, wind speed and the circulation patterns in the embayments (identified from the model velocity profiles) and determined the critical wind speeds and values for B, at which either wind stress or buoyancy forces became the dominant force driving the exchange.

Results

Surface meteorological conditions, heat flux, and water temperature at the lake interior

Air temperature, wind speed, and wind direction collected at the LDS during the field experiment are shown on Fig. 2a,b. The experiment began with a 6-d cooling period with increasing wind speeds, followed by 3 d of increasing air temperatures and decreasing wind speeds. The cooling of the air above the reservoir was greatest on the first 2 d of the experiment; the maximum air temperature above the reservoir fell by 2.4°C from 26.7°C to 24.3°C and the minimum air temperature fell by 3.3°C from 22.2°C to 18.9°C. Air temperatures remained relatively steady and mild during the day (23.5–24.6°C) and cool at night (16.5–18.2°C) for the next 4 d.

For the first 6 d of the experiment, the wind measured in the interior of the reservoir was gentle to fresh (typically within the range of 3.5–10.7 ms^{-1}) and predominantly from the south-southeast or southeast. The wind speed decreased from approximately 7 ms^{-1} to 5 ms^{-1} over the first 4 d. On the fifth and sixth days the wind speed was slightly higher, reaching peaks of 9.4 ms^{-1} and 8.2 ms^{-1} in the morning of the 2 d respectively.

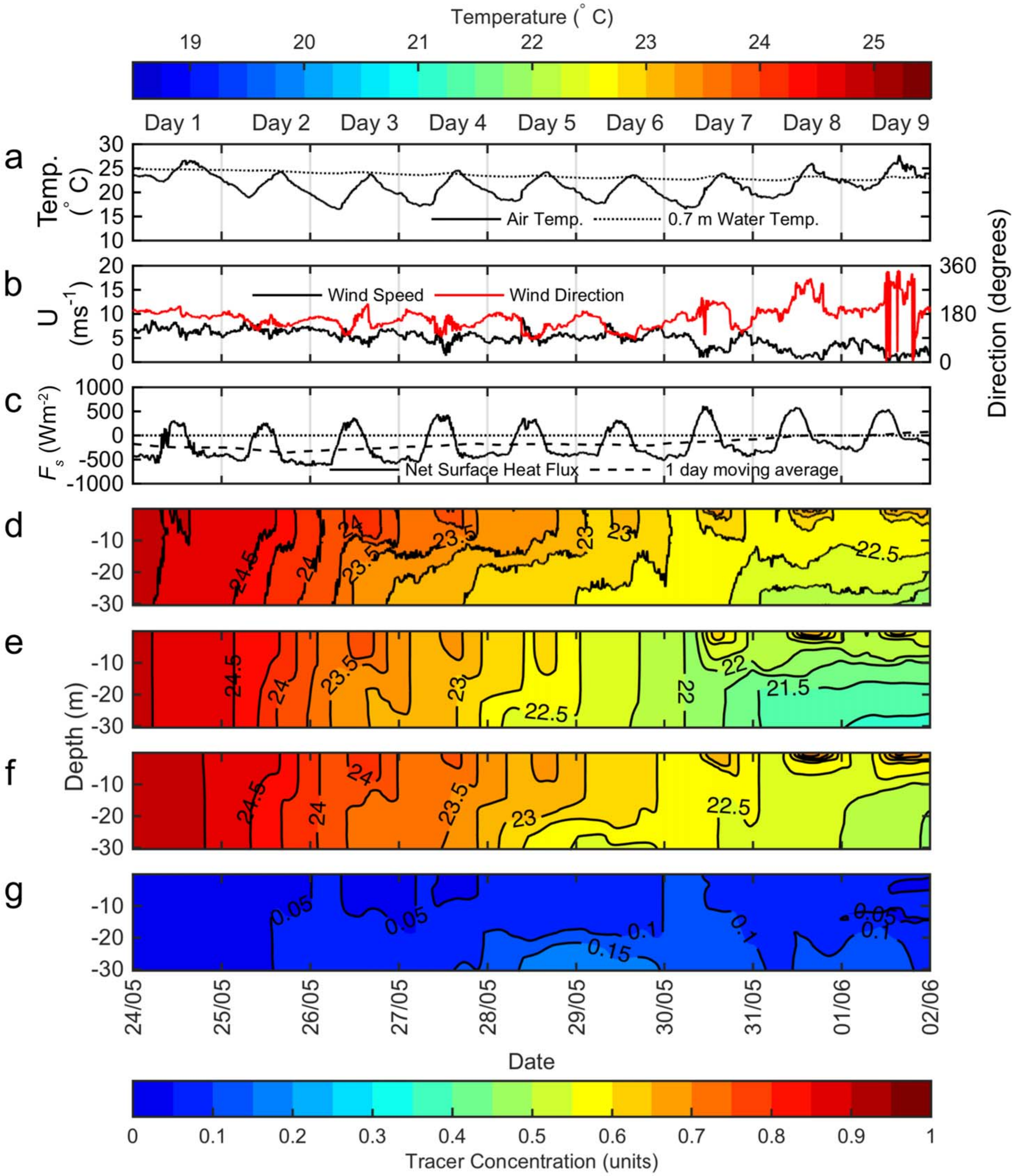

Fig. 2. Conditions at the Lake Diagnostic System (LDS) site; (**a**) air temperature above the water surface and water surface temperature at 0.7 m, (**b**) wind speed (U) and wind direction, (**c**) net surface heat flux (F_s) and 1 d moving average of F_s into the surface layer, (**d**) observed water temperatures, (**e**) simulated water temperatures under Scenario 1, (**f**) simulated water temperatures under Scenario 4, and (**g**) simulated tracer concentration under Scenario 4. The contour interval in panels **d**, **e**, and **f** is 0.25°C.

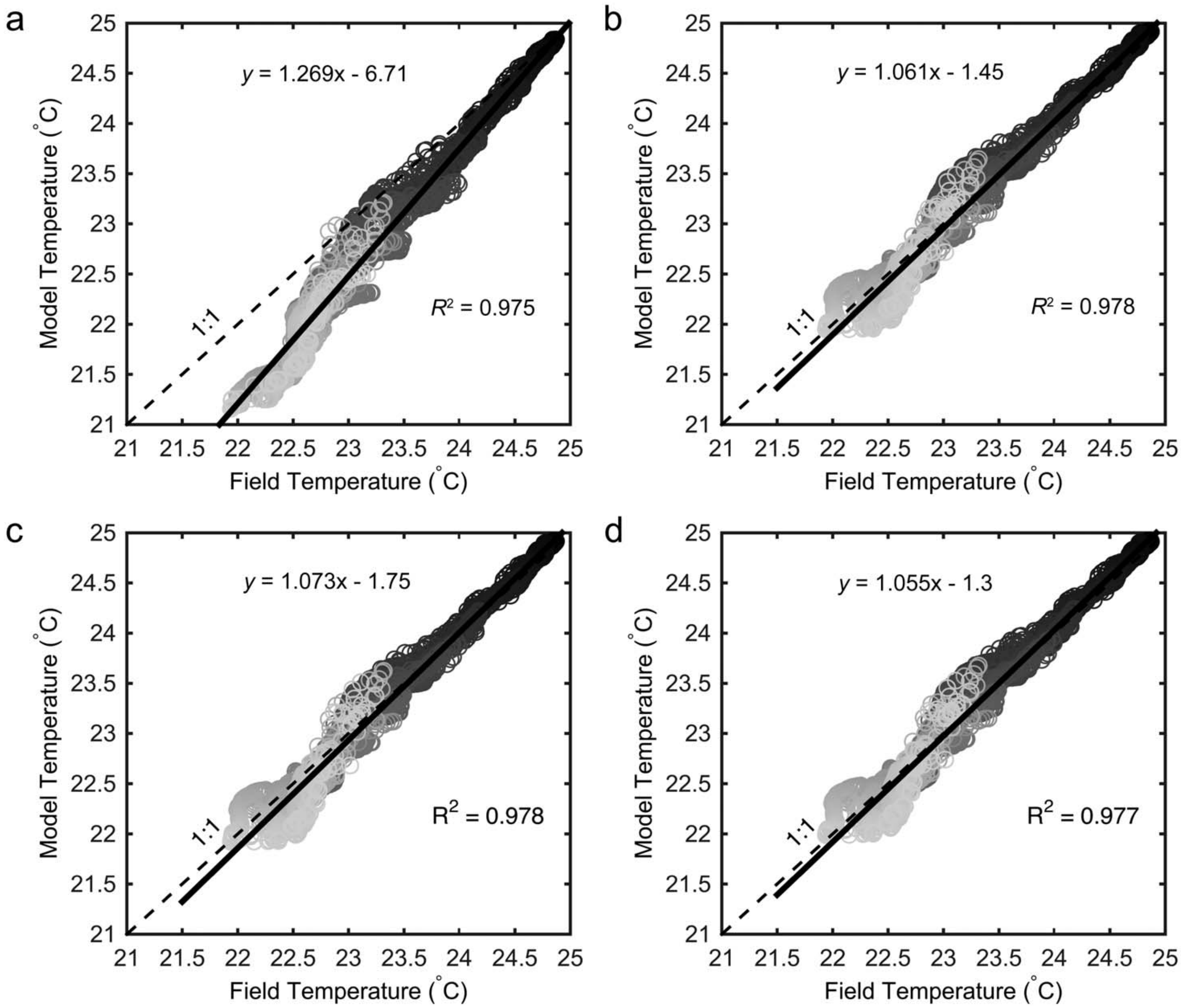

Fig. 3. Comparison of all simulated and observed temperatures at the Lake Diagnostic System (LDS), under Scenarios 1 to 4, (**a**–**d**). Shading reflects time within the simulation period (dark at the beginning and light at the end). Comparison points were taken every hour for each thermistor for the entire simulation period. The solid line indicates the regression line; the dashed line indicates the 1 : 1 regression line.

The effective heat flux into the surface layer, F_s (Fig. 2c) had an average maximal value of 423 Wm^{-2} and an average minimal value of -518 Wm^{-2}. Due to the large sensible and latent heat losses resulting from the cool and windy conditions during the first 6 d of the experiment, the daily average heat flux was negative (-352 Wm^{-2} to -172 Wm^{-2}) causing the reservoir to cool. The cooling was greatest on the first 2 d of the experiment and the surface water temperature at the LDS fell by approximately 0.7°C from 24.8°C to 24.1°C between the first and the second day (Fig. 2d).

On the first day of the experiment the water temperatures at the LDS (Fig. 2d) were almost isothermal with a difference of less than 0.2°C recorded between the surface and bottom thermistors. On the second day of the experiment the temperature difference increased to more than 0.4°C and the isotherms became slightly slanted indicating an intrusion of cool water along the bottom of the reservoir. This cool bottom layer became more obvious over the next few days and, as will be discussed later, its origin was an underflow from the reservoir embayments. Over the morning of the seventh

Table 2. Average root mean squared error (RMSE) for simulated and measured temperature data at the Lake Diagnostic System (LDS) and indicative embayment exchange flow rates and flushing times for different model scenarios.

	Scenario 1	Scenario 2	Scenario 3	Scenario 4
	RMSE (°C)			
	0.500	0.137	0.146	0.136
	Exchange flow rate, Q (m^3 d^{-1})			
Cooee Creek	1.41×10^7	1.39×10^7	1.39×10^7	1.21×10^7
Ulysses Bay	1.81×10^6	1.81×10^6	1.83×10^6	1.79×10^6
	Flushing time (days)			
Cooee Creek	9.41	9.63	9.63	11.04
Ulysses Bay	9.41	9.38	9.28	9.50

day of the experiment, the cold bottom layer was removed by night-time cooling and mixing, which caused the lake water temperature to decrease to 22.6°C. Cooler water with a temperature below 22.5°C was observed again later that night, below 15 m depth.

During the last 3 d of the experiment the maximum air temperature increased by 3.8°C from 23.9°C to 27.7°C. The minimum air temperature also increased by 3.9°C from 16.5°C to 20.4°C. The wind decreased in speed, typically to a gentle breeze below 4 ms^{-1} and changed in direction to predominantly from the south-southwest.

Diurnal heating of the upper water column was strongest on the last 3 d of the experiment due to the warmer and calmer conditions. The daily average heat flux from the reservoir began to increase on the seventh day of the experiment and became positive midway through the afternoon of the eighth day and on the last day reached a maximum of 75 Wm^{-2}. The temperature of the surface layer increased by 0.15°C from 23.05°C to 23.25°C between the middle of the seventh and ninth days, but the cold bottom layer became more prominent, cooling by 0.6°C, from 22.6°C to 22.0°C. At the end of the experiment the temperature difference between the surface and bottom thermistors was greater than 1°C.

Model performance

The observed and modelled water temperatures at the LDS were compared for Scenarios 1 and 4 (Fig. 2d–f) and regression plots of the observed and simulated temperatures for Scenarios 1 to 4 and calculation of the average RMSE indicated increased performance of each subsequent simulation (Fig. 3; Table 2). Under Scenario 1, overcooling of the bottom layer in the ELCOM simulation caused the data to diverge from the 1 : 1 line increasingly as the simulation progressed (Fig. 3a, slope = 1.269, intercept = −6.71). Incorporating wind sheltering (Scenario 2) led to a model prediction of temperature that was still systematically too low (Fig. 3b), with the regression line steeper than the 1 : 1 ideal regression line (slope = 1.061) and the intercept below zero (−1.45). Adding shading by macrophytes to the reduced wind scenario, but without vegetation drag (Scenario 3), increased the degree of overcooling (Fig. 3c, slope = 1.073, intercept = −1.75). Finally, the inclusion of vegetation drag by macrophytes in the littoral zones (Scenario 4) improved model performance within the lake interior (Fig. 3d, slope = 1.055, intercept = −1.30), but this was only slightly better than if macrophytes had not been included at all. The calculation of the average RMSE (Table 2) yielded an error of less than 0.15°C for Scenarios 2 to 4 compared to 0.5°C for the original model set up with full wind and no macrophytes (Scenario 1).

Statistical analysis to compare simulated and observed temperatures in the embayments was not conducted because there were far fewer observed data at these locations than at the LDS. Nonetheless, a time series plot of the available field and model results shows the depth-averaged temperature at the 2.5 m and 5 m depth contours in the creek channels of the embayments predicted by the model, was generally within 1°C of the field results (Fig. 4). The inclusion of macrophytes improved model performance in the Cooee Creek embayment but not in Ulysses Bay.

In Cooee Creek, the averaged difference between the depth-averaged observed and modelled temperatures for Scenario 2 (reduced wind, no macrophytes) at 5 m depth was 0.6°C (Fig. 4a) and the difference ranged between 0.86°C cooler to 0.92°C warmer. When macrophytes (shading and drag) were added to the model (Scenario 4) the average difference was reduced to 0.42°C and the range was between 0.71°C degrees cooler to 0.48°C warmer. At 2.5 m water depths, the depth-averaged modelled temperatures were on average 0.61°C cooler than those observed. When macrophytes were added to the model, this difference was less than 0.28°C.

In Ulysses Bay, the depth-averaged model temperature was 0.28°C cooler than the observed temperature at 5 m depth and 0.75°C cooler at 2.5 m depth (Fig. 4b). When macrophytes were added to the model (Scenario 4) the difference between the observed and modelled temperatures increased by approximately 0.2°C at both depths, due to the amplified cooling.

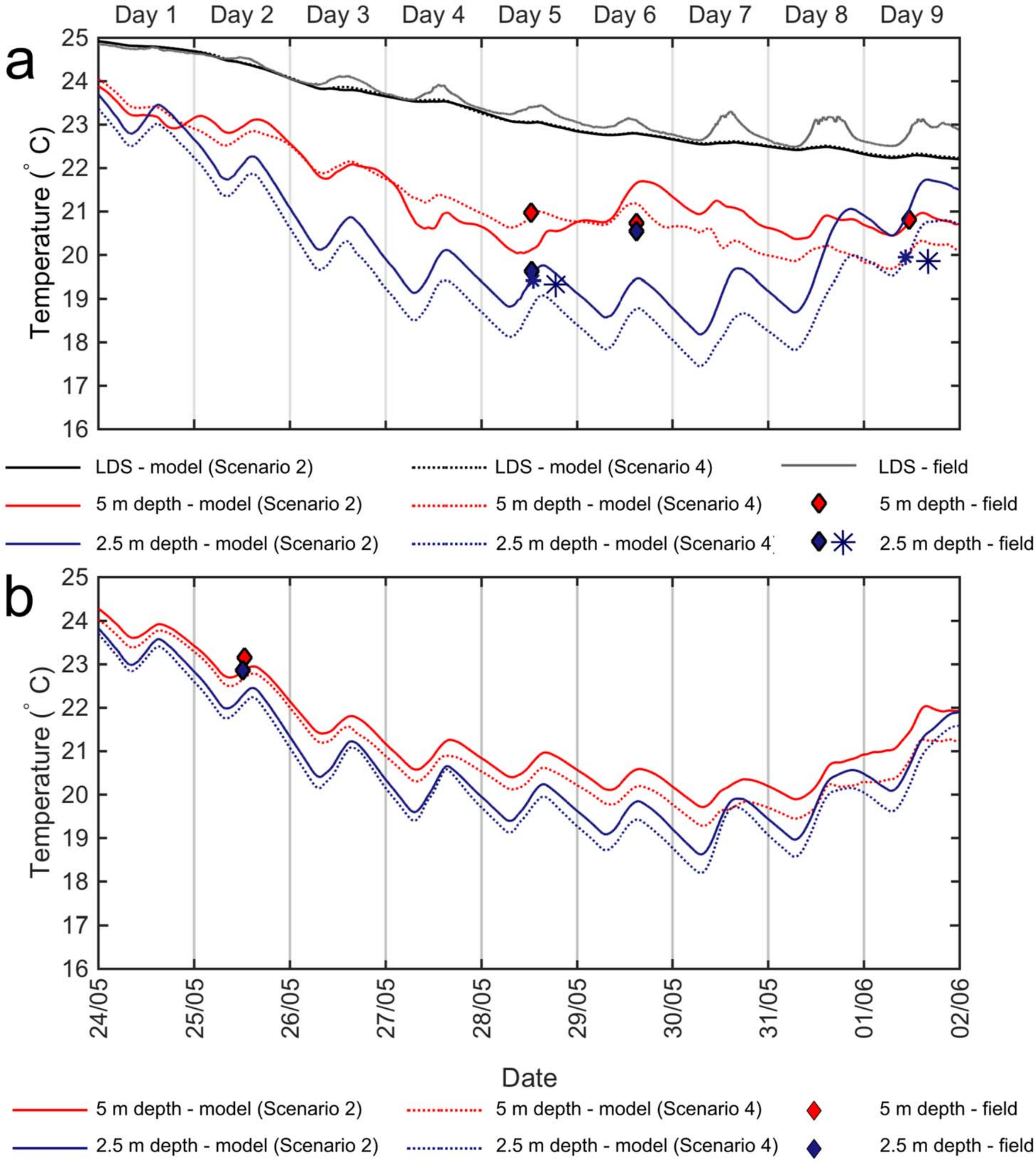

Fig. 4. Comparison of depth-averaged water temperatures at the lake interior (Lake Diagnostic System) and (**a**) at the 2.5 m and 5 m depth contours along Cooee Creek and (**b**) along the submerged river channel in Ulysses Bay. Model results without macrophytes (Scenario 2) and with macrophytes (Scenario 4) are shown as a line. Field observations are shown as stars (within macrophyte beds) or diamonds (elsewhere).

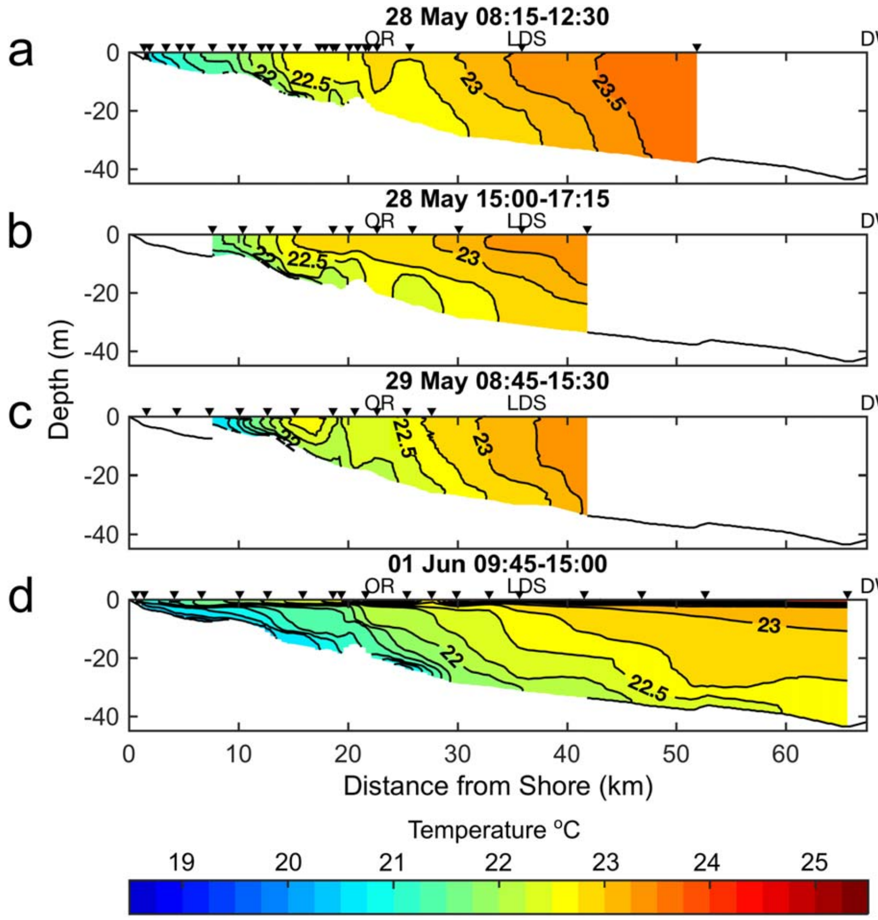

Fig. 5. Spatial variation of measured temperatures along the Cooee Creek transect (*see* Fig. 1) in (**a**) the morning and (**b**) the afternoon of the fifth day of the experiment; (**c**) on the sixth day of the experiment and (**d**) on the last day of the experiment. The transect follows the creek channel, then the Ord River (OR) and the distance is measured from the shore. Triangles indicate profile locations, including the Lake Diagnostic System (LDS), and dam wall (DW). The contour interval is 0.25°C.

There was a good agreement between measured and modelled water level for all Scenarios and the water level calculated from the water budget (not shown).

Exchange between the embayments and the lake interior

At the beginning of the experiment the depth-averaged modelled water temperature at the 2.5 m depth contour of the Cooee Creek embayment was approximately 1.5°C cooler than at the LDS for the best scenario (Scenario 4) (Fig. 4a). The model predicted a slightly smaller temperature difference (1.1°C cooler) if macrophytes were not included in the model (Scenario 2). Similar temperature differences were observed between the interior and the littoral zone of Ulysses Bay (Fig. 4b). Both embayments cooled faster than the lake interior during the first 6 d of the experiment. For Scenarios 2 and 4, the modelled temperature in the shallow parts of the embayments fell to below 19°C by the morning of the seventh day, and was more than 4°C cooler than at the LDS (Fig. 4a,b).

During the warmer and calmer conditions between the seventh and the last day of the experiment, the model scenarios with and without macrophytes (Scenarios 2 and 4) and the field results, all showed water temperatures in the embayments increasing faster than the interior (Fig. 4). By midday of the last day of the experiment, water temperatures in the shallow embayments rose above 20°C (Fig. 4a,b). Strong diurnal stratification was evident in the temperature transect taken on the last day of the experiment (Fig. 5d). Despite this heating trend toward the end of the experiment, the embayments were always cooler than the interior water.

During the field experiment, the submerged, attached macrophyte *Hydrilla* sp. was observed growing along the perimeter of the embayments, mostly where the water was less than 2.5 m deep; there were however some areas in this zone without any macrophyte growth. The macrophytes were typically dense, often forming thick surface canopies, shading the underlying water. The depth-averaged field temperatures within the macrophyte canopies in the Cooee

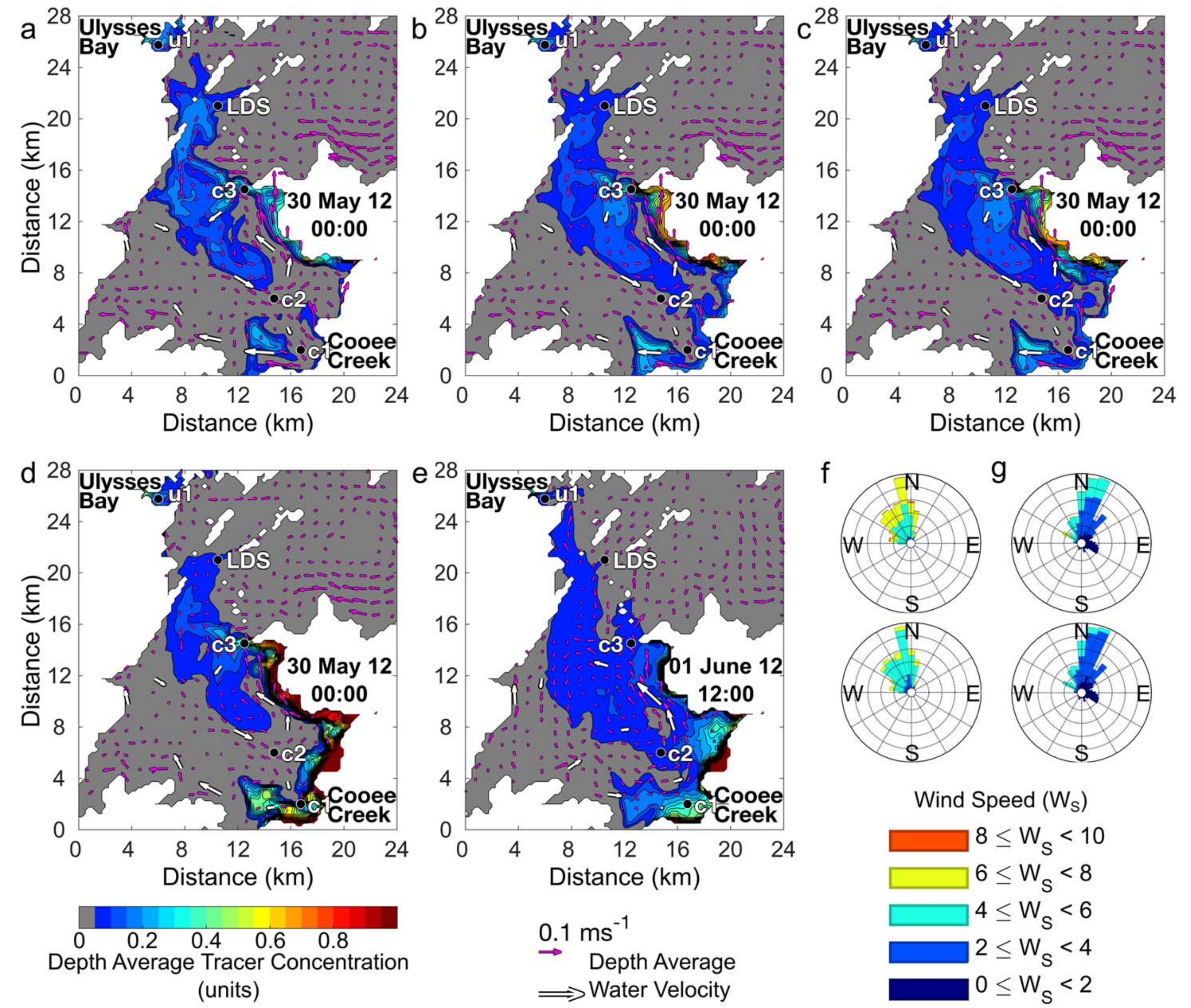

Fig. 6. Simulated depth-averaged velocity vectors and tracer concentrations (**a–d**) under Scenarios 1 to 4 six days after the tracer was introduced in the embayments (< 5 m depth), and (**e**) for Scenario 4 on the last day of the simulation, 8.5 d after the tracer was released; (**f**) wind across the first 6 d of the experiment and (**g**) wind across the last 3 d. The winds shown are for the reduced wind conditions used under Scenarios 2 to 4. Points c1, c2, c3, and u1 are locations of model velocity profiles shown in Fig. 8.

Creek embayment were approximately 0.22°C colder than in the clear water at the same location (Fig. 4a) and the water was up to 1.2°C colder at the bottom of the profile.

Over time, the isotherms in the Cooee Creek embayment became increasingly slanted downward, from the shore of the reservoir toward the interior, and increasingly compressed near the reservoir surface (Fig. 5). The cool bottom layer at the LDS (Fig. 2d) and the slope of the isotherms in the temperature transects (Fig. 5), indicate an underflow of cool, dense water arising from the reservoir embayments, and flowing along the drowned river channels toward the center of the reservoir. The simulated tracer introduced in the shallows at the start of the experiment in model Scenario 4 (Fig. 2g), confirmed than the cool water at the LDS originated from the embayments. Similar concentrations of tracer were observed at the LDS under the other model scenarios. The observed compressed isotherms toward the end of the experiment also suggest the occurrence of a return surface flow from the interior (Fig. 5d). On day 6 of the experiment, the model velocity vectors and tracer concentrations show a north-westerly current along the northern bank of the Cooee Creek embayment and a south-easterly return flow into the middle of the embayment (Fig. 6); it appears this circulation pattern is due to the development of a topographic gyre. When wind stress acts along a long and narrow basin of varying depth, a double gyre pattern develops with coastal currents in the direction of the wind stress and a return flow in the center of the basin in the opposite direction (Csanady 1982). In contrast, a flow pattern characteristic of a topographic gyre was not observed in Ulysses Bay.

Discussion

Forces driving exchange in the embayments

Strong horizontal temperature gradients between the shore and the interior of lakes result when differential cooling is intensified by synoptic-scale weather systems (Curtarelli et al. 2014). In Lake Argyle, the horizontal temperature gradient increased over a cooling period lasting several days and reached a maximum of more than 4°C. This is approximately double the strength of the gradient observed in reservoirs subject only to diurnal patterns of night-time cooling (James and Barko 1991a,b) and it was observed that the cooler temperatures in the embayments persisted throughout the 9-d field experiment. The buoyancy force created by this temperature gradient would drive a warm overflow into the embayments if there were no opposing wind stress. During the first 6 d of the experiment, winds were predominantly from a south-southeast or southeasterly direction (Fig. 2b). The Cooee Creek embayment is aligned with its shallow end pointing toward the southeast, therefore the shear force acted in opposition to the buoyancy force in this embayment, directing an offshore surface flow.

The calculation of the dimensionless parameter (B) using Eq. 4 and the horizontal temperature gradient and reduced wind speed from model Scenario 4, indicated that the shear force was greater than the buoyancy force in the Cooee Creek embayment only on the first 2 d of the experiment, and even then it was less than 2.5 times greater (Fig. 7a). For most of the rest of the experiment the buoyancy force was greater than the shear force. The relative magnitude of the buoyancy force was greatest on the last 3 d of the experiment due to warming of the embayment (Figs. 4, 5), and because the shear force directed along the embayment became weaker as the wind speed decreased and the predominant direction changed to south-southwesterly (Fig. 2b), i.e., toward the northern shore of the embayment.

Ulysses Bay is aligned with its shallow end pointing toward the west (Fig. 1) so the winds on the first 6 d of the experiment would have driven a surface flow out of the embayment in the same direction as the buoyancy-driven flow. Calculation of B for Scenario 4 showed that for the duration of the experiment, the shear force in this embayment either acted in the same direction to the buoyancy force or the buoyancy force was of a greater magnitude (Fig. 7a). The shear force was also smaller in Ulysses Bay than in the Cooee Creek embayment because the wind had a smaller fetch to act over.

Despite the relatively strong buoyancy forces resulting from differential cooling in Lake Argyle, the modelled tracer and velocities indicated that for most of the experiment, wind and the resulting topographic gyre had major influences on circulation within the Cooee Creek embayment in all of the model scenarios. The circulation in this embayment was classified as gyre driven when the model velocity was predominantly in north-westerly direction along the northern bank of the embayment, and south-easterly along the creek channel into the middle of the embayment. For the first 6 d of the experiment the velocity profiles of the Cooee Creek embayment were in the direction of the gyre circulation pattern (Fig. 8a–c). Under these conditions the ratio of the shear and buoyancy force, averaged over 6 h (B_{6h}), was greater than 0.5 (Fig. 7b). This occurred when the 6 h averaged wind speed (U_{6h}) rose above a critical value of $U_s = 4.5$ ms^{-1} (Fig. 7b). A 6-h average was used to define the critical values for wind speed and the ratio of the shear and buoyancy force to remove irregular, short-term variations that are too brief to influence circulation patterns in the reservoir while still capturing the effect of diurnal variability in the wind and heat flux. This time period was scaled from the typical velocities of wind and buoyancy driven flow in the embayments ($\sim$ 0.05 ms^{-1}) and the length scale of the embayments (several km). The critical wind speed at which the gyre circulation pattern became dominant is similar to the wind speeds of 4 ms^{-1} observed to erode a buoyant surface water outflow in the forebay of a shallow wetland (Nepf and Oldham 1997).

Nepf and Oldham estimated that opposing wind speeds as low as 0.5 ms^{-1} may be sufficient to arrest buoyancy driven flow but we found that gyre dominated flows did not occur when B_{6h} was less than 0.1 or when U_{6h} was below a critical speed $U_b = 2.4$ ms^{-1} (Fig. 7b). For these conditions, modelled velocity structures often suggested buoyancy-driven flows dominated (*see* Fig. 8d,e). The circulation in the Cooee Creek embayment was classified as buoyancy-driven if the model velocity was predominantly in a north-westerly direction at the bottom, and south-easterly at the surface along the creek channel. The circulation in Ulysses Bay was classified as buoyancy-driven if the model velocity was predominantly in an easterly direction at the bottom, and westerly at the surface along the creek channel into the middle of the embayment. Velocity profiles indicative of purely buoyancy driven flow only occurred when B_{6h} was less than 0.1, which only happened on in the late afternoon on the last 2 d of the experiment, under the reduced wind scenarios in the Cooee Creek embayment but on several occasions in Ulysses Bay (Fig. 7b). When wind sheltering was not included, often the model did not predict buoyancy-dominated flows in the Cooee Creek embayment.

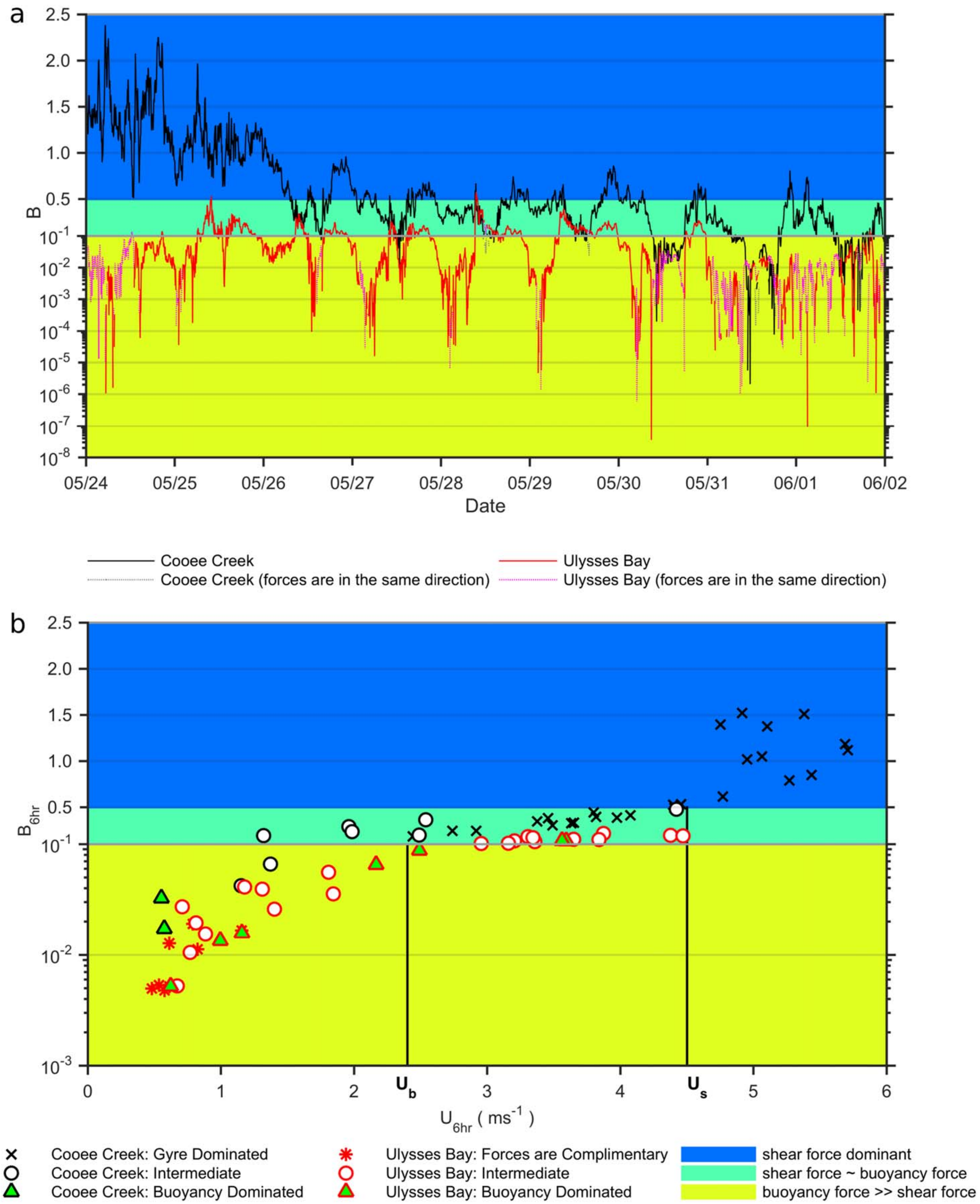

Fig. 7. (**a**) Times series of the ratio of the shear and buoyancy forces (B) and (**b**) the relationship between the ratio averaged over 6 h (B_{6h}) with the 6 h averaged wind speed (U_{6h}) and simulated velocity structures in the Cooee Creek embayment and Ulysses Bay under Scenario 4. U_s and U_b represents critical values for U_{6h} at which the model velocity indicates either shear or buoyancy forces become the dominant influence on the embayment circulation.

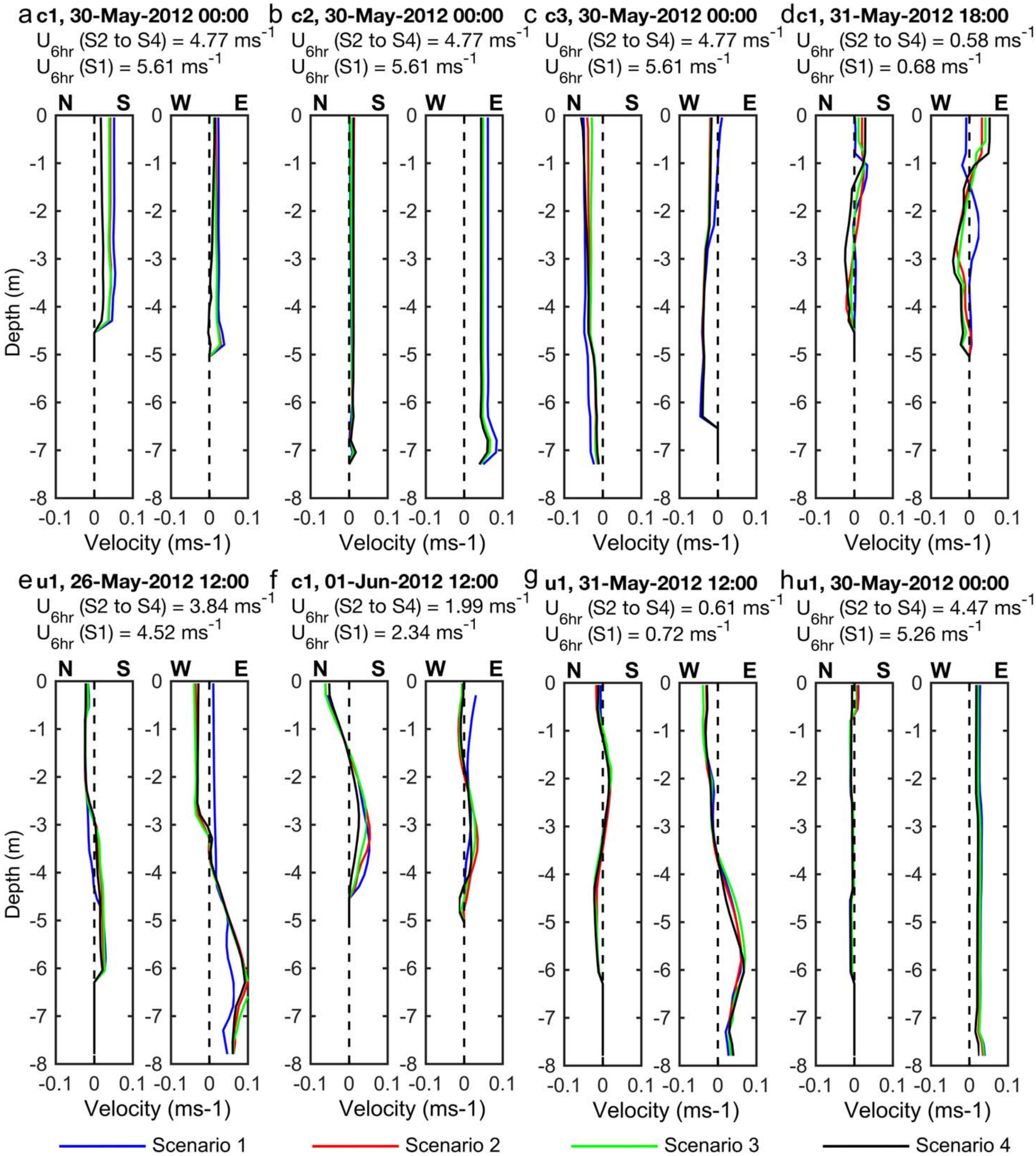

Fig. 8. Instantaneous model velocity profiles showing topographic gyre dominated flow (**a**,**b**) along the creek channel and (**c**) along the northern bank of the Cooee Creek embayment, a two layered flow structure indicating a density driven flow along the creek channels of (**d**) the Cooee Creek embayment and (**e**) Ulysses Bay and flow structures resulting from the likely interaction of buoyancy and/or wind driven forces and topography in the creek channels of (**f**) Cooee Creek and (**g**,**h**) Ulysses Bay. The locations of the velocity profiles (c1, c2, c3, u1) are shown on Fig. 6. The 6-h averaged wind speed (U_{6h}) is shown at the top of each profile.

Frequently the model velocity profiles in both embayments did not have the shape expected of flow driven purely by the topographic gyre or buoyancy forces (Fig. 7b). These cases were classified as "intermediate" because it appeared that the circulation was influenced by the interaction between both wind stress and buoyancy forces. For example, in the Cooee Creek embayment, as the topographic gyre weakened on the last 3 d of the experiment, often a complex velocity structure with two or more layers occurred (*see* e.g., Fig. 8f) and it is likely that this circulation pattern resulted from the interaction between the buoyancy driven flow, the wind and the residual circulation from the topographic gyre.

In Ulysses Bay, the shear force was often in the same direction as the buoyancy force and the circulation was classified as "complimentary" in these cases. A topographic gyre was not observed but the velocity output by the model in Ulysses Bay was not always in the direction of the predominant wind or in the direction expected of purely buoyancy driven exchange flow. Sometimes the model velocity profiles showed a multi-layered structure (Fig. 8g) or showed an easterly flow out of the embayment (Fig. 8h). This indicates that even in an embayment where wind stress is relatively small or even complementary to the buoyancy force, circulation patterns are still complicated by the combined effects of wind and topography.

Velocity structures that appeared to be influenced by both buoyancy and wind forcing occurred when U_{6h} was as low as 0.6 ms^{-1} (Fig. 7b); this supports conclusions from early numerical analyses by Cormack et al. (1975) who suggested that even a relatively small surface stress can have a large impact on the velocity structure within a shallow cavity. We identified an intermediate zone between $0.1 < B_{6h} < 0.5$ and $2.4 < U_{6h} < 4.5$ where there was evidence from the velocity structure, that the flow was driven sometimes by buoyancy forces, occasionally by the topographic gyre and often by a mix of both of these mechanisms (Fig. 7b).

Influence of the topographic gyre, wind sheltering, and macrophytes on the exchange

Gyres can trap water in the littoral zone of lake embayments (Razmi et al. 2013) but the tracer simulations show that the topographic gyre in the Cooee Creek embayment only temporarily trapped water. It is likely that the underflow of cool water along the river channel in the Cooee Creek embayment would have been inhibited by the shoreward, south-easterly current created by the gyre, but the tracer simulations show that the north-westerly current along the northern bank of the embayment eventually transported littoral water into the reservoir interior (Fig. 6). As discussed above and shown in Fig. 8, the embayment velocity structures predicted under the different model scenarios were quite different, indicating that wind sheltering and macrophytes were important influences on embayment circulation. To gain a further insight into these processes, an indicator of the rate of exchange between the embayments and the reservoir interior, Q, was estimated for each of the model scenarios as:

$$Q = V\frac{dC}{dt}\frac{1}{-C_0} \tag{5}$$

where V is the total volume of the embayment, $\frac{dC}{dt}$ is the change in the model tracer concentration in the embayment over the duration of the experiment (9 d) and C_0 is the model tracer concentration in the embayment when it was first introduced. The embayment boundaries were defined to encompass water depths less than 5 m. Equation 5 is derived from the mass balance equations for advective transport (Schnoor 1996) and is a simple indicator of the average exchange flow rate over time t. It assumes the tracer is well mixed throughout the embayment, which will not be the case in reality as time progresses, and it assumes no tracer mass inflow even though some may return into the embayment in the exchange flow. Despite these assumptions, inspection of how Q changes with forcing conditions can be useful.

The calculation of Q for each of the model scenarios (Table 2) highlighted that vegetation drag was the only parameter that had a noticeable effect on reducing the exchange between the embayments and the interior in Lake Argyle. When the effect of vegetation drag was included in the model (Scenario 4), Q fell by 12.8% in the Cooee Creek embayment, the estimated flushing time of the embayment increased from approximately 9.5–11 d (Table 2) and the spread of the tracer was noticeably reduced (Fig. 6). This supports previous findings that vegetative drag controlled exchange between the rooted aquatic canopies and open water (Zhang and Nepf 2009) and increased flushing timescales in sheltered wetlands (Oldham and Sturman 2001). Vegetation drag reduced Q by only 2.3% in Ulysses Bay but this was still larger than the changes in Q from wind sheltering and macrophyte shading. Reducing the wind field in the model to account for sheltering (Scenario 2) reduced Q by just 1.6% in the Cooee Creek embayment and 0.33% in Ulysses Bay. Adding shading by macrophytes to this scenario without drag (Scenario 3) had almost no effect in both embayments (Table 2).

Considerations for lake and reservoir modelling

Comparison of the continuous cumulative distribution function of B, which gives the probability that B will take a value less than or equal to B, for each of the model scenarios (Fig. 9) highlights that the model scenario without any wind sheltering (Scenario 1) had far more values of B above 0.5 than the other model scenarios. There were much fewer values of B below 0.1 for Scenario 1 compared to the scenarios with reduced wind and macrophytes (Scenarios 3 and 4). The density of values of B below 0.1 for Scenario 2 (reduced

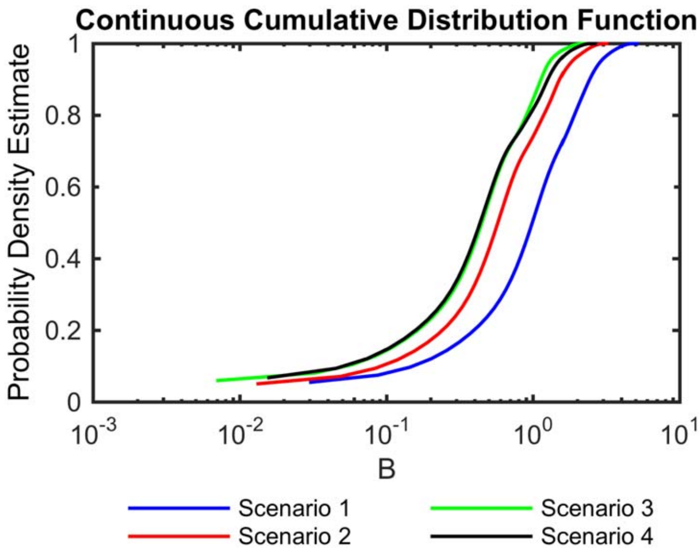

Fig. 9. Probability density estimates for the ratio of the shear and buoyancy forces (*B*) under Scenarios 1 to 4.

wind, no macrophytes) was between Scenario 1 and Scenarios 3 and 4. This comparison of *B* values across the different scenarios suggests that without wind sheltering included, the model was more likely to show that flows would be dominated by a topographic gyre, and less likely to predict buoyancy-dominated flows. The results also highlight that when macrophytes were included in littoral zones, the model would be more likely to predict buoyancy-dominated flows.

The model prediction of the water temperature in the interior of the reservoir was improved by reducing wind speed across the whole lake to account for wind sheltering. This wind sheltering can also alter the flow structure out of the embayments. The presence of macrophytes in the model noticeably reduced the exchange between the interior and the embayments by increasing vegetation drag, however did not have much influence on the temperature structure at the LDS. These findings highlight the importance of capturing processes occurring in the littoral zone in numerical models, even though their importance may not be always be detected by simply examining temperature structure in the interior. The modeller should be wary of not considering these processes even if an adequate match with field results arises, because the errors associated with incorrect assumptions and set up can cancel each other out. For example, a lower RMSE (0.25°C) resulted when Scenario 1 was run without correction for non-neutral atmospheric stability (not shown) because the resulting underestimation of the heat losses was offset by the overestimation of heat losses due to the lack of wind sheltering.

In the model investigation presented here, a wind-sheltering coefficient was estimated based on a spatially averaged topography, and was applied uniformly across the lake surface. However the topography around the lake is much higher on the western side so the wind field over the reservoir will be variable. If the lake was forced by a spatially and temporally variable wind field, as suggested by Rueda et al. (2005), the different dynamics of the embayments based on their alignment to the prevailing wind and degree of sheltering could be examined in more detail. Further investigation is needed to assess the ability of different numerical models to capture circulation features in embayments with complex morphometry. In addition, higher spatial resolution observational data is required to validate the impact of complex topographically controlled boundary layers on lake temperatures and circulation (Huber et al. 2008).

Implications for lake and reservoir ecology and management

Large fluxes of particulate phosphorus from the littoral to the pelagic zone have been observed in other reservoirs under differential cooling (James and Barko 1991) and in buoyant wind-driven surface plumes (George 2000). In these studies, phosphorus concentrations were much higher in the littoral zone, due to dissolved phosphorus release from oxic sediments at high pH due to macrophyte photosynthetic activity. Little is known about the sediment nutrient dynamics in the littoral zones of Lake Argyle, but profile data showed high pH and > 100% oxygen saturation in the embayment shallows, suggesting that similar phosphorus dynamics could occur in the reservoir. Underflows generated during differential cooling, with high dissolved phosphorus concentrations, can increase productivity of vertically migrating phytoplankton species (James et al. 1992). If this underflow was mixed into the surface waters, such as occurred on day 7 of our experiment, phytoplankton communities in the surface water have the opportunity to take advantage of the resulting increased nutrient concentrations.

Embayments or sidearms of lakes or reservoirs may also receive anthropogenic chemicals from wastewater discharge, stormwater or inflows from rivers or streams draining urban or agricultural catchments. Studies have shown that the flushing time of lake embayments influences water and sediment quality within the embayments (Razmi et al. 2014). Harmful algal blooms may occur in a system if the flushing rate is lower than the growth rate of the algal species (Garcon et al. 1986). Given the estimated flushing time of the embayments is $\sim$ 10 d (Table 2), which is greater than the typical doubling times of freshwater phytoplankton of ~ 1 d^{-1} (Reynolds 2006) it is unlikely wind and buoyancy driven exchange will prevent algal blooms in the embayments of Lake Argyle however they may help to reduce bloom severity.

Aquaculture often takes place in the embayments of lakes and reservoirs and has been trialled previously in Lake Argyle, but without success due to an outbreak of pathogenic bacteria (Glencross et al. 2007). Water exchange rates in the vicinity of the aquaculture operation influence the local impact of pathogens and diseases (Choi and Lee 2004). The flushing rate is also a key component in determining the capacity of the receiving environment to assimilate aquaculture effluent and is evaluated to determine the potential impacts on water quality (Hamblin and Gale 2004). The calculation of Q, as an indicator of exchange flows, suggests the Cooee Creek embayment and Ulysses Bay had similar flushing times during the field experiment (Table 2) but the flushing times may be higher or lower in other embayments. A comparison of Q across embayments, under different water levels, meteorological conditions and macrophyte densities, could facilitate decisions on where to place activities such as aquaculture.

In lakes and reservoirs with significant shallow regions, gravity currents from differential cooling may produce stratification in the cool season when they would be otherwise well mixed (Wells and Sherman 2001). The transport of cool water from the littoral zone to the interior of Lake Argyle caused the temperature difference between the surface and bottom waters at the center of the reservoir to increase from less than 0.2°C to more than 1°C during the 9 d field experiment. Such stratification in the cool season may lead to more frequent blooms of phytoflagellates and buoyant cyanobacteria that are more often associated with strongly stratified water columns in the warmer season (Sherman et al. 2001). Indeed Talling (1963) observed vertical stratification of temperature, dissolved oxygen, silica, and diatoms in a tropical lake, that persisted long after cooling had finished; gravity currents generated by differential cooling in the littoral zones may have been the origin of the observed stratification.

Conclusion

Field observations in a tropical reservoir with a complex topography and vegetated littoral zone were complemented by higher temporal and spatial resolution model results. We have identified, critical ratios of wind stress and buoyancy forces and critical wind speeds at which horizontal exchange between the embayments and the interior is driven predominantly by (1) the wind and a resulting topographic gyre or (2) density differences. Despite the relatively strong buoyancy forces resulting from synoptic-scale differential cooling, a simple buoyancy-driven flow was rarely observed because this required buoyancy forces to be an order of magnitude greater than shear forces. This was only common when the 6-h averaged wind speed in the direction of the embayment (U_{6h}) fell below 2.4 ms^{-1}. Instead we found that wind dominated the circulation most of the time in the largest embayment, when the ratio of the shear and buoyancy force, averaged over 6 h (B_{6h}) was greater than 0.5 which occurred when U_{6h} was greater than 4.5 ms^{-1}. Otherwise, a complex circulation was observed, most likely due to interactions between buoyancy-driven flow, the wind and a topographic gyre (2.4 ms$^{-1} < U_{6h} < 4.5$ ms^{-1}). The relative magnitude of the forces in the embayments was influenced by how they were aligned in relation to the direction of the prevailing wind but even in an embayment where wind stress was either relatively small or complementary to the buoyancy-forced flows, circulation patterns were still complicated by the combined effects of wind and bathymetry. The transport of cool water from the littoral zone to the interior through wind- and buoyancy-driven exchange can be important for the ecology of a tropical lake because it facilitates the exchange of nutrients and contaminants between the two zones and sets up stratification in the cooler months when it may not be expected. Both of these processes have the potential to influence phytoplankton dynamics and the distribution of dissolved constituents throughout the water body.

The model prediction of temperature in the interior of Lake Argyle was improved by reducing wind speed across the whole lake to account for wind sheltering; we expect this could be further improved by forcing the lake with a spatially variable wind field. It is also important to include wind sheltering in the model so that periods when flows are dominated by a topographic gyre are not overestimated, and the significance of buoyancy-dominated flows is not underestimated. Although model results showed that macrophytes did not have much influence on the temperature structure at the LDS, vegetation drag reduces the flushing of the embayments and when they are included the model is more likely to predict buoyancy-dominated flows. Therefore, it is important to consider processes occurring in the littoral zone in numerical models, even though their significance may not be always be detected by simply examining temperature structure in the interior. Even if an adequate match with field results arises, the modeller should still be wary of not considering all the processes that effect the heat budget and horizontal transport within a lake, because the errors associated with incorrect assumptions and set up, can cancel each other out.

References

Ali, A., and C. J. Lemckert. 2009. A traversing system to measure bottom boundary layer hydraulic properties. Estuar. Coast. Shelf Sci. **83**: 425–433. doi:10.1016/j.ecss.2009.04.017

Andratottir, H. O., and H. M. Nepf. 2001. Impact of exchange flows on wetland flushing. Water Resour. Res. **37**: 3265–3273. doi:10.1029/2001WR000257

Choi, K. W., and J. H. W. Lee. 2004. Numerical determination of flushing time for stratified water bodies. J. Mar. Syst. **50**: 263–281. doi:10.1016/j.jmarsys.2004.04.005

Chung, S. W., M. R. Hipsey, and J. Imberger. 2009. Modelling the propagation of turbid density inflows into a stratified lake: Daecheong Reservoir, Korea. Environ. Model. Softw. **24**: 1467–1482. doi:10.1016/j.envsoft.2009.05.016

Cormack, D. E., G. P. Stone, and L. G. Leal. 1975. The effect of upper surface conditions on convection in a shallow cavity with differentially heated end-walls. Int. J. Heat Mass Transf. **18**: 635–648. doi:10.1016/0017-9310(75)90275-6

Csanady, G. 1982. Circulation in the coastal ocean. Springer.

Curtarelli, M. P., E. H. Alcantara, C. D. Renno, and J. L. Stech. 2014. Physical changes within a large tropical hydroelectric reservoir induced by wintertime cold front activity. Hydrol. Earth Syst. Sci. **18**: 3079–3093. doi:10.5194/hess-18-3079-2014

Dixon, R., and D. Palmer. 2010. Lake Argyle sedimentation - 2006 survey. Department of Water, Perth, Australia.

Farrow, D. E., and J. C. Patterson. 1994. Daytime circulation and temperature structure in a reservoir sidearm. Int. J. Heat Mass Transf. **37**: 1957–1968. doi:10.1016/0017-9310(94)90335-2

Farrow, D. E. 2012. Periodically driven circulation near the shore of a lake. Environ. Fluid Mech. **13**: 243–255. doi:10.1007/s10652-012-9261-4

Fozdar, F. M., G. J. Parker, and J. Imberger. 1985. Matching temperature and conductivity sensor response characteristics. J. Phys. Oceanogr. **15**: 1557–1569. doi:10.1175/1520-0485(1985)015 < 1557:MTACSR>2.0.CO;2

Garcon, V. C., K. D. Stolzenbach, and D. M. Anderson. 1986. Tiday flushing of an estuarine embayment subject to recurrent dinoflagellate blooms. Estuaries **9**: 179–187. doi:10.2307/1352129

George, D. G. 2000. Remote sensing evidence for the episodic transport of phosphorus from the littoral zone of a thermally stratified lake. Freshw. Biol. **43**: 571–578. doi:10.1046/j.1365-2427.2000.00540.x

Glencross, B., S. Percival, B. Jones, and J. Hughes. 2007. Kimberley Sustainable Regions Program. Sustainable development of barramundi cage aquaculture at Lake Argyle. Final report to Fisheries Research and Development Corporation on Project No. 2003/026. Fisheries Research Report No. 168, Department of Fisheries, Western Australia.

Hamblin, P. F., and P. Gale. 2002. Water quality modeling of caged aquaculture impacts in Lake Wolsey, North Channel of Lake Huron. J. Great Lakes Res. **28**: 32–43. doi:10.1016/S0380-1330(02)70560-1

Hodges, B. R., J. Imberger, A. Saggio, and K. B. Winters. 2000. Modeling basin-scale internal waves in a stratified lake. Limnol. Oceanogr. **45**: 1603–1620. doi:10.4319/lo.2000.45.7.1603

Hodges, B. R., and C. Dallimore. 2013. Estuary, Lake and Coastal Ocean Model: ELCOM v2.2 Science Manual. Centre for Water Research, University of Western Australia.

Huber, A., G. N. Ivey, G. Wake, and C. E. Oldham. 2008. Near-surface wind-induced mixing in a mine lake. J. Hydraul. Eng. **134**: 1464–1472. doi:10.1061/(asce)0733-9429(2008)134:10(1464)

Imberger, J. 1977. A preliminary study of the dynamics of Lake Argyle: Second report on the physical monitoring program of the holomictic tropical lake. Univ. of Berkley.

Imberger, J. 1985. Thermal characteristics of standing waters: An illustration of dynamic processes. Hydrobiologia **125**: 7–29. doi:10.1007/BF00045923

Imberger, J. 2004. A Lake Diagnostic System for managing lakes and reservoirs. Water Resour. Impact **6**: 7–10.

Imberger, J., and J. C. Patterson. 1990. Physical limnology. Adv. Appl. Mech. **27**: 303–475. doi:10.1016/S0065-2156(08)70199-6

Imberger, J., and R. Head. 1994. Measurement of turbulent properties in a natural system, p. 1–20. In C. A. Pugh [ed.], Fundamentals and advancements in hydraulic measurements and experimentation. ASCE Publications.

James, W. F., and J. W. Barko. 1991a. Littoral-pelagic phosphorus dynamics during nighttime convective circulation. Limnol. Oceanogr. **36**: 949–960. doi:10.4319/lo.1991.36.5.0949

James, W. F., and J. W. Barko. 1991b. Estimation of phosphorus exchange between littoral and pelagic zones during nighttime convective circulation. Limnol. Oceanogr. **36**: 179–187. doi:10.4319/lo.1991.36.1.0179

James, W. F., W. D. Taylor, and J. W. Barko. 1992. Production and vertical migration of Ceratium hirundinella in relation to phosphorus availability in Eau Galle Reservoir, Wisconsin. Can. J. Fish. Aquat. Sci. **49**: 694–700. doi:10.1139/f92-078

James, W. F., J. W. Barko, and H. L. Eakin. 1994. Convective water exchanges during differential cooling and heating: Implications for dissolved constituent transport. Hydrobiologia **294**: 167–176. doi:10.1007/BF00016857

Johns, B. 1983. Physical oceanography of coastal and shelf seas. Elsevier Science Publishers.

Kimberley Aquaculture Development Strategy: Lake Argyle Barramundi Aquaculture Industry Strategic Environmental Review. 1999. LeProvost, Dames and Moore Report for Environmental Protection Authority, Perth, Australia.

Leon, L. F., J. P. Antenucci, Y. R. Rao, and C. McCrimmon. 2012. Summary performance of the estuary and lake computer model (ELCOM): Application in the Laurentian and other Great Lakes. Water Qual. Res. J. Canada **47**: 252–267. doi:10.2166/wqrjc.2012.022

Leonard, B. P. 1991. The ULTIMATE conservative difference scheme applied to unsteady one-dimensional advection. Comput. Methods Appl. Mech. Eng. **88**: 17–74. doi:10.1016/0045-7825(91)90232-U

Lewis, W. M. 1996. Tropical lakes: How latitude makes a difference, p. 43–64. *In* F. Schiemer and K. T. Boland [eds.], Perspectives in tropical limnology. SPB Academic Publishing.

Lin, Y. T. 2015. Wind effect on diurnal thermally driven flow in vegetated nearshore of a lake. Environ. Fluid Mech. **15**: 161–178. doi:10.1007/s10652-014-9368-x

Lin, Y. T., and C. H. Wu. 2015. Effects of a sharp change of emergent vegetation distributions on thermally driven flow over a slope. Environ. Fluid Mech. **15**: 771–791. doi:10.1007/s10652-014-9382-z

Lorke, A., F. Peeters, and E. Bäuerle. 2006. High-frequency internal waves in the littoral zone of a large lake. Limnol. Oceanogr. **51**: 1935–1939. doi:10.4319/lo.2006.51.4.1935

Lorke, A., L. Umlauf, and V. Mohrholz. 2008. Stratification and mixing on sloping boundaries. Geophys. Res. Lett. **35**: L14610. doi:10.1029/2008GL034607

Lövstedt, C. B., and L. Bengtsson. 2008. Density-driven current between reed belts and open water in a shallow lake. Water Resour. Res. **44**: 13. doi:10.1029/2008WR006949

Machado, D. A., C. L. Marti, and J. Imberger. 2014. Influence of microscale turbulence on the phytoplankton of a temperate coastal embayment, Western Australia. Estuar. Coast. Shelf Sci. **145**: 80–95. doi:10.1016/j.ecss.2014.04.018

MacIntyre, S., J. Romero, and G. W. Kling. 2002. Spatial-temporal variability in surface layer deepening and lateral advection in an embayment of Lake Victoria, East Africa. Limnol. Oceanogr. **47**: 656–671. doi:10.4319/lo.2002.47.3.0656

Macintyre, S., J. R. Romero, G. M. Silsbe, and B. M. Emery. 2014. Stratification and horizontal exchange in Lake Victoria, East Africa. Limnol. Oceanogr. **59**: 1805–1838. doi: 10.4319/lo.2014.59.6.1805

Markfort, C. D., A. L. S. Perez, J. W. Thill, D. A. Jaster, F. Porté-Agel, and H. G. Stefan. 2010. Wind sheltering of a lake by a tree canopy or bluff topography. Water Resour. Res. **46**: 1–13. doi:10.1029/2009WR007759

Marti, C. L., and J. Imberger. 2006. Dynamics of the benthic boundary layer in a strongly forced stratified lake. Hydrobiologia **568**: 217–233. doi:10.1007/s10750-006-0111-6

Marti, C. L., and J. Imberger. 2008. Exchange between littoral and pelagic waters in a stratified lake due to wind-induced motions: Lake Kinneret, Israel. Hydrobiologia **603**: 25–51. doi:10.1007/s10750-007-9243-6

Marti, C. L., J. Imberger, L. Garibaldi, and B. Leoni. 2016. Using time scales to characterize phytoplankton assemblages in a deep subalpine lake during the thermal stratification period: Lake Iseo, Italy. Water Resour. Res. **52**: 1762–1780. doi:10.1002/2015WR017555

Monismith, S. G., J. Imberger, and M. L. Morison. 1990. Convective motions in the sidearm of a small reservoir. Limnol. Oceanogr. **35**: 1676–1702. doi:10.4319/lo.1990.35.8.1676

Nepf, H. M., and C. E. Oldham. 1997. Exchange dynamics of a shallow contaminated wetland. Aquat. Sci. **59**: 193–213. doi:10.1007/s000270050008

Oldham, C. E., and J. J. Sturman. 2001. The effect of emergent vegetation on convective flushing in shallow wetlands: Scaling and experiments. Limnol. Oceanogr. **46**: 1486–1493. doi:10.4319/lo.2001.46.6.1486

Peel, M. C., B. L. Finlayson, and T. A. McMahon. 2007. World map of the Köppen-Geiger climate classification updated. Hydrol. Earth Syst. Sci. **11**: 1633–1644. doi: 10.1127/0941-2948/2006/0130

Peeters, F., D. Finger, M. Hofer, M. Brennwald, D. M. Livingstone, and R. Kipfer. 2003. Deep-water renewal in Lake Issyk-Kul driven by differential cooling. Limnol. Oceanogr. **48**: 1419–1431. doi:10.4319/lo.2003.48.4.1419

Pokorný, J., and J. Květ. 2004. Aquatic plants and lake ecosystems, p. 309–340. *In* P. E. O'Sullivan and C. S. Reynolds [eds.], The lakes handbook: Limnology and limnetic ecology, v. 1. Blackwell Science.

Public Works Department Western Australia Nautical Chart: 53375. 1982. Lake Argyle, Side A, 1: 100 000.

Rattray, M., and D. Hansen, Jr. 1962. A similarity solution for circulation in an estuary. J. Mar. Res. **20**: 121–133.

Razmi, A. M., D. A. Barry, R. Bakhtyar, N. Le Dantec, A. Dastgheib, U. Lemmin, and A. Wüest. 2013. Current variability in a wide and open lacustrine embayment in Lake Geneva (Switzerland). J. Great Lakes Res. **39**: 455–465. doi:10.1016/j.jglr.2013.06.011

Razmi, A. M., D. A. Barry, U. Lemmin, F. Bonvin, T. Kohn, and R. Bakhtyar. 2014. Direct effects of dominant winds on residence and travel times in the wide and open lacustrine embayment: Vidy Bay (Lake Geneva, Switzerland). Aquat. Sci. **76**: 59–71. doi:10.1007/s00027-013-0321-8

Reynolds, C. S. 2006. The ecology of phytoplankton. Cambridge Univ. Press.

Roget, E., J. Colomer, X. Casamitjana, and J. E. Llebot. 1993. Bottom currents induced by baroclinic forcing in Lake Banyoles (Spain). Aquat. Sci. **55**: 206–227. doi:10.1007/BF00877450

Rueda, F. J., and S. G. Schladow. 2003. Dynamics of large polymictic lake II: Numerical simulations. J. Hydraul. Eng. **129**: 92–101. doi:10.1061/(ASCE)0733-9429(2003)129:2(92)

Rueda, F. J., S. G. Schladow, S. G. Monismith, and M. T. Stacey. 2003. Dynamics of large polymictic lake. I: Field observations. J. Hydraul. Eng. **129**: 82–91. doi:10.1061/(ASCE)0733-9429(2003)129:2(82)

Rueda, F. J., and E. A. Cowen. 2005. Exchange between a freshwater embayment and a large lake through a long, shallow channel. Limnol. Oceanogr. **50**: 169–183. doi: 10.4319/lo.2005.50.1.0169

Rueda, F. J., S. G. Schladow, S. G. Monismith, and M. T. Stacey. 2005. On the effects of topography on wind and the generation of currents in a large multi-basin lake. Hydrobiologia **532**: 139–151. doi:10.1007/s10750-004-9522-4

Sand-Jensen, K. 2003. Drag and reconfiguration of freshwater macrophytes. Freshw. Biol. **48**: 271–283. doi:10.1046/j.1365-2427.2003.00998.x

Schnoor, J. L. 1996. Environmental modelling. Fate and Transport of Pollutants in Water, Air and Soil, New York. John Wiley & Sons.

Sherman, B., P. Ford, P. Hatton, J. Whittington, D. Green, D. S. Baldwin, R. Oliver, R. Shiel, J. vanBerkel, R. Beckett, L. Grey, & B. Mayer. 2001. The Chaffey Dam Story. CRC for Freshwater Ecology, Canberra, Australia.

Spera, D. A., and T. R. Richards. 1979. Modified power law equations for vertical wind profiles. Conference and workshop on wind energy characteristics and wind energy siting (June 1979), Portland, OR, USA.

Talling, J. F. 1963. Origin of stratification in an African rift lake. Limnol. Oceanogr. **8**: 68–78. doi:10.4319/lo.1963.8.1.0068

Talling, J. F., and J. L. Lemoalle. 1998. Ecological dynamics of tropical inland waters. Cambridge Univ. Press.

Tanino, Y. 2004. Aquatic gravity currents through emergent vegetation. Master's thesis, Massachusetts Institute of Technology.

Tanino, Y. 2012. Water exchange between littoral zone and open lake water, p. 869–872. *In* L. Bengtsson, R. W. Herschy, and R. W. Fairbridge [eds.], Encyclopedia of lakes and reservoirs. Springer.

Verburg, P., and J. P. Antenucci. 2010. Persistent unstable atmospheric boundary layer enhances sensible and latent heat loss in a tropical great lake: Lake Tanganyika. J. Geophys. Res. Atmos. **115**: 1–13. doi:10.1029/2009JD012839

Verburg, P., J. P. Antenucci, and R. E. Hecky. 2011. Differential cooling drives large-scale convective circulation in Lake Tanganyika. Limnol. Oceanogr. **56**: 910–926. doi:10.4319/lo.2011.56.3.0910

von Karman, T. 1921. Über laminare und turbulente Reibung. Angew. Math. Mech. **1**: 233–252. doi:10.1002/zamm.19210010401

Wells, M. G., and B. Sherman. 2001. Stratification produced by surface cooling in lakes with significant shallow regions. Limnol. Oceanogr. **46**: 1747–1759. doi:10.4319/lo.2001.46.7.1747

Wetzel, R. G. 2001. Limnology: Lake and river ecosystems, 3rd ed. Academic Press.

Yu, P., J. C. Patterson, and C. W. Lei. 2015. A scaling analysis of transient natural convection in a reservoir model induced by iso-flux heating. J. Fluid Mech. **764**: 219–249. doi:10.1017/jfm.2014.697

Zhang, X., and H. M. Nepf. 2009. Thermally driven exchange flow between open water and an aquatic canopy. J. Fluid Mech. **632**: 227–243. doi:10.1029/2007WR006676

Acknowledgments

We acknowledge the contribution of two anonymous reviewers for comments that helped improve this contribution. We thank the following institutions for providing data: land based air temperature and climate data, Australian Bureau of Meteorology (BoM); upstream flow data, Department of Water; water level, hydropower and regulated releases, Water Corporation and bathymetric data, Department of Transport. Roger Head, Greg Attwater, Carol Lam, Lee Goodyear and Angus Stewart are acknowledged for their support in the acquisition and processing of field data. We thank Kevin Boland for sharing fascinating insights in tropical lakes and Chris Dallimore for help with revision of the ELCOM source code. The Kimberley Development Commission and the Centre for Water Research (CWR) funded this work. B.L.W. was supported by Australian Postgraduate Award, an Ad Hoc CWR Scholarship, a University Postgraduate Award and a UWA Safety Net Top-Up Scholarship.

Conflict of Interest

None declared.

Submitted 16 September 2016
Revised 12 December 2016
Accepted 10 January 2017

Associate editor: Francisco Rueda